An *LC* Squared-Compensated Inductive Power Transfer System With Misalignment Tolerance and Constant-Current Output

Yiming Zhang, *Senior Member, IEEE*, Hongmin Tang, Zhiwei Shen, Yizhan Zhuang, *Member, IEEE*, and Zhongqi Li, *Member, IEEE*

***Abstract*—Inductive power transfer enjoys the advantages of convenience and adaptability to various application scenarios. However, the coil misalignment normally cannot be avoided in practical applications, which can cause a dramatic decline of the mutual inductance and a sharp fluctuation of the output. To solve this issue, this article proposes an inductor–capacitor (*LC*) squared-compensated topology based on three integrated and decoupled transmitting coils. The simple series compensation is adopted on the secondary side, forming an *LC* squared series topology with a constant-current (CC) output. The receiving coil has couplings with the first and third transmitting coils. Thus, the output is related to the two mutual inductances, which can be optimized for a smooth output against misalignment with a proper design of the magnetic couplers. The mathematical model is established and analyzed. The experimental results obtained from the prototype reveal that the output fluctuates less than 6% from the central to the boundary positions. Also, a CC output independent of the load is realized. Compared with previous methods, the proposed method is a low-cost solution to achieve misalignment tolerance.**

***Index Terms*—Constant current (CC), inductive power transfer (IPT), *LC* squared compensation, misalignment tolerance, wireless power transfer (WPT).**

I. Introduction

THE rapid increase in the market share of electric vehicles (EVs) has led to an increasing interest in the EV charging methods. The traditional plug-in charging method is the most common way to charge EVs. However, it has the disadvantages of inconvenience, intervention of human labor, and possible electric shocks, especially in rainy or snowy weather. Inductive power transfer (IPT), as an emerging charging technology, can overcome the disadvantages of the plug-in charging method [1], [2], [3]. Compared with plug-in charging, IPT is more automotive, aesthetic, and suitable for various weather conditions [4]. Meanwhile, users can avoid touching the possibly dirty and heavy cable, significantly improving the convenience of charging. The technology is currently used in EVs [5], autonomous underwater vehicles [6], [7], drones [8], and railway transport system [9], [10].

However, one of the obstacles facing the IPT system is the misalignment between the transmitting and receiving coils [11], [12], which is inevitable for human parking. Misalignment will lead to a fluctuation of the mutual inductance, affecting the output and safe operation of the system. In terms of the offset direction, the EV position can be easily adjusted along the front–rear direction but is challenging along the door–door direction. Thus, the misalignment tolerance along the door–door direction is critical.

To achieve misalignment tolerance, different approaches can be adopted. Adding a dc–dc converter on the secondary side can regulate the impedance for antioffset purposes, but it results in extra components, loss, and cost. A common category is using control strategies, such as pulse density modulation control or pulse frequency modulation control, to regulate the transmission power and maintain relatively stable output characteristics under misalignment conditions [13], [14]. However, the system may lose the soft-switching operation, and the complexity will be increased.

A dual-channel inductance–capacitance–capacitance-series topology and a delicate coil structure were proposed to achieve offset tolerance performance [15]. Combining multiple windings to achieve the relative constancy of the equivalent mutual inductance is simple and reliable. Wang et al. [16] proposed a reconfigurable topology where two antiparallel windings are connected in series. This results in the equivalent mutual inductance being the difference between the two mutual inductances. The adoption of the antiparallel windings can smooth the variation of coupling coefficients at different positions by reducing the coupling coefficients at the center position and enhancing the coupling coefficients at the boundary positions [17].

Another strategy is using hybrid and reconfigurable topologies to achieve a stable output [18]. The hybrid topology is

Manuscript received 16 September 2023; revised 21 November 2023; accepted 21 December 2023. Date of publication 28 December 2023; date of current version 16 February 2024. This work was supported in part by the National Natural Science Foundation of China under Grant 52107183 and in part by the Natural Science Foundation of Fujian Province under Grant 2022J06011. Recommended for publication by Associate Editor K. Ngo. *(Corresponding authors: Yizhan Zhuang; Yiming Zhang.)*

Yiming Zhang, Hongmin Tang, Zhiwei Shen, and Yizhan Zhuang are with the School of Electrical Engineering and Automation, Fuzhou University, Fuzhou 350108, China (e-mail: zym@fzu.edu.cn; 220127089@fzu.edu.cn; 210127138@fzu.edu.cn; zyz_joe@fzu.edu.cn).

Zhongqi Li is with the College of Railway Transportation, Hunan University of Technology, Zhuzhou 412007, China (e-mail: lizhongqi@hnu.edu.cn).

Color versions of one or more figures in this article are available at https://doi.org/10.1109/TPEL.2023.3347721.

Digital Object Identifier 10.1109/TPEL.2023.3347721

characterized by the fact that the system's equivalent mutual inductance is a function of more than one mutual inductance. In [19], a hybrid combination of *LCC* and S both on the primary and secondary sides was proposed to smooth the output. The reconfigurable IPT system with misalignment tolerance was proposed in [20]. In [21], a hybrid IPT system was proposed, consisting of paralleling S–S and *LCC–LCC* compensation networks on the primary and secondary sides. A detuned S–S topology was proposed in [22], which can maintain relatively smooth output for a variable coupling coefficient. In addition, a reformed *LCC* compensation topology was proposed in [23], which can achieve a relatively stable output for misalignment conditions. Reconfiguring topologies using relays is also an effective way [24], [25]. Another purpose of using reconfigurable topology is to achieve constant-voltage (CV) or constant-current (CC) output. However, it is inevitable to add switching devices to realize topology reconfiguration. New compensation networks and magnetic coupler structures should be explored to further improve the misalignment tolerance performance, on the condition that no extra components are introduced on the secondary side to maintain high power density and low cost in the EV [26].

This article proposes an IPT system with secondary-side series compensation and primary-side inductor–capacitor (*LC*) squared compensation to realize misalignment tolerance and a CC output [31]. The proposed three coils on the primary side are integrated and decoupled from each other. A prototype is implemented to validate the proposal. The rest of this article is organized as follows. In Section II, the mathematical model is built and theoretical analysis is conducted to describe the proposed IPT system. The design method and decoupling principle of the coil structures are described in detail, and specific design flowcharts and optimization results are given. The performance of the proposed *LC* squared IPT system for a variable load and against pad misalignment is verified in Section III with the implemented 1.3-kW prototype. Finally, Section IV concludes this article.

II. Proposed IPT System

A. LC *Squared Compensation*

The proposed *LC* squared-compensated IPT system is depicted in Fig. 1(a). The inverter operating at 85 kHz consists of four power MOSFETs. V_{INV} (U_I) and V_{REC} (U_O) are the inverter and rectifier dc (ac) voltages, respectively. R_L is the load resistance. L_M is the self-inductance of Coil X ($1 \le X \le 4$). C_X and I_X are the compensating capacitance and the coil current, respectively. M_{14} (M_{34}) is the mutual inductance between Coil 1 (3) and Coil 4. The equivalent circuit is shown in Fig. 1(b). R_{EQ} is the equivalent load resistance. R_X is the equivalent series resistance (ESR) of Coil X. Based on the fundamental harmonic approximation, U_I, U_O, and R_{EQ} can be expressed as follows:

$$\begin{cases} U_I = \frac{2\sqrt{2}}{\pi} V_{\mathrm{INV}} \\ U_O = \frac{2\sqrt{2}}{\pi} V_{\mathrm{REC}} \\ I_4 = \frac{\pi}{2\sqrt{2}} I_{\mathrm{REC}} \\ R_{\mathrm{EQ}} = \frac{8}{\pi^2} R_L. \end{cases} \tag{1}$$

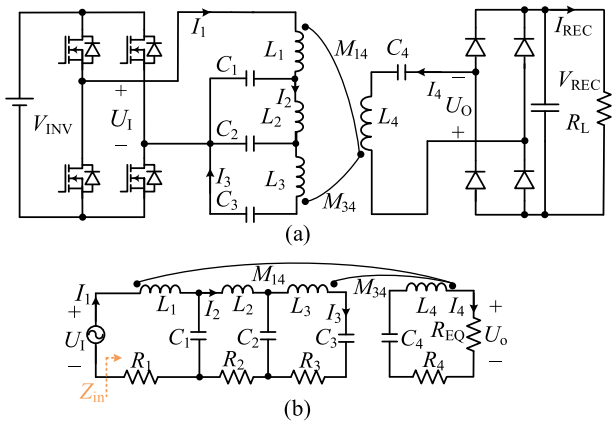

Fig. 1. Proposed *LC* squared-compensated IPT system for misalignment tolerance. (a) Topology. (b) Equivalent circuit.

The system resonant angular frequency can be expressed as follows:

$$\omega_0^2 = \frac{1}{L_1 C_1} = \frac{1}{L_2 \frac{C_1 C_2}{C_1 + C_2}} = \frac{1}{L_3 \frac{C_2 C_3}{C_2 + C_3}} = \frac{1}{L_4 C_4}. \tag{2}$$

Define

$$K_C = \frac{C_2}{C_1}. \tag{3}$$

The compensation capacitors can be calculated as follows:

$$\begin{cases} C_1 = \frac{1}{\omega_0^2 L_1} \\ C_2 = K_C C_1 \\ C_3 = \frac{1}{\omega_0^2 \left(L_3 - \frac{L_1}{K_C} \right)} \\ C_4 = \frac{1}{\omega_0^2 L_4}. \end{cases} \tag{4}$$

L_1 and C_1 constitute the first resonant loop. C_1, L_2, and C_2 form the second resonant loop. C_2, L_3, and C_3 constitute the third resonant loop. On the secondary side, L_4 and C_4 form the fourth. At ω_0, based on Kirchhoff's voltage law, the model can be established as

$$\begin{bmatrix} R_1 & -1/j\omega_0 C_1 & 0 & -j\omega_0 M_{14} \\ -1/j\omega_0 C_1 & R_2 & -1/j\omega_0 C_2 & 0 \\ 0 & -1/j\omega_0 C_2 & R_3 & j\omega_0 M_{34} \\ -j\omega_0 M_{14} & 0 & j\omega_0 M_{34} & R_4 + R_{\mathrm{EQ}} \end{bmatrix} \begin{bmatrix} I_1 \\ I_2 \\ I_3 \\ I_4 \end{bmatrix} = \begin{bmatrix} U_I \\ 0 \\ 0 \\ 0 \end{bmatrix}. \tag{5}$$

Ignoring the ESRs in (5), the currents can be obtained as

$$\begin{cases} I_1 = \frac{R_{\mathrm{EQ}} U_{\mathrm{I}}}{\omega_0^2 M_{\mathrm{EQ}}^2} \\ I_2 = -\frac{j\omega_0 M_{34} C_2 U_{\mathrm{I}}}{M_{\mathrm{EQ}}} \\ I_3 = \frac{K_C R_{\mathrm{EQ}} U_{\mathrm{I}}}{\omega_0^2 M_{\mathrm{EQ}}^2} \\ I_4 = \frac{j U_{\mathrm{I}}}{\omega_0 M_{\mathrm{EQ}}} \end{cases} \tag{6}$$

where M_{EQ} is the equivalent mutual inductance, defined as

$$M_{\mathrm{EQ}} = M_{14} + K_C M_{34}. \tag{7}$$

M_{EQ} is the summation of M_{14} and M_{34} multiplied by a coefficient K_C. M_{14} and M_{34} can be designed as two monotonically changing curves against misalignment so that their summation can remain stable. K_C offers another design degree of freedom to keep M_{EQ} relatively stable, guaranteeing a good misalignment tolerance performance. The value of K_C can be adjusted by controlling the ratio of C_1 and C_2. There is an optimal K_C value for a specific set of coil turns and dimensions. The optimal K_C can be selected according to the simulation results and the design guidelines.

Define the fluctuation of M_{EQ} as

$$F_M = \frac{M_{\mathrm{EQ-max}} - M_{\mathrm{EQ-min}}}{M_{\mathrm{EQ-max}} + M_{\mathrm{EQ-min}}} \times 100\% \tag{8}$$

where $M_{\mathrm{EQ\text{-}max}}$ is the maximum value of M_{EQ} and $M_{\mathrm{EQ\text{-}min}}$ is the minimum value. F_M can be utilized to denote the misalignment performance of the designed magnetic couplers.

From (6), I_4 is independent of R_{EQ}, indicating that the system achieves a CC output. Also, I_4 is determined by M_{EQ}, which can be designed to be stable against misalignment with proper magnetic coupler design. Therefore, the output current can be maintained relatively stable.

From (6), the input impedance Z_{IN} is

$$Z_{\mathrm{IN}} = \frac{\omega_0^2 M_{\mathrm{EQ}}^2}{R_{\mathrm{EQ}}}. \tag{9}$$

Z_{IN} is resistive, indicating that zero phase angle (ZPA) can be achieved.

The output power and the dc–dc efficiency can be expressed as follows:

$$P_O = |I_4|^2 R_{\mathrm{EQ}} = \frac{R_{\mathrm{EQ}} U_I^2}{\left(\omega_0^2 M_{\mathrm{EQ}}\right)^2} \tag{10}$$

$$\eta = \frac{|I_4|^2 R_{\mathrm{EQ}}}{|I_1|^2 R_1 + |I_2|^2 R_2 + |I_3|^2 R_3 + |I_4|^2 (R_4 + R_{\mathrm{EQ}})}. \tag{11}$$

B. Magnetic Couplers

The proposed coil structure is shown in Fig. 2. The primary-side pad size is 390 × 400 mm, and the secondary side is 300 × 300 mm. The thickness of both ferrites is 2.5 mm. All the windings are wounded by Litz wires with a diameter of 4.25 mm. There are three coils on the primary side. Coil 2 is placed beneath the ferrite plate, as it is not involved in the coupling process. Coil 1 is a unipolar coil with an antiparallel winding placed above the ferrite plate to smooth the coupling coefficient variation. The two windings are 12 turns and 8 turns, respectively. Two eight-turn unipolar coils arranged above Coil 1 form Coil 3. Coil 1 and Coil 3 have been specifically designed to overlap with each other to achieve decoupling. This coil arrangement is to ensure that the variation trends of M_{13} and M_{34} are opposite with offset so that M_{EQ} in (7) can maintain relatively stable. K_C can be regulated by adjusting the value of L_2 to help obtain this target.

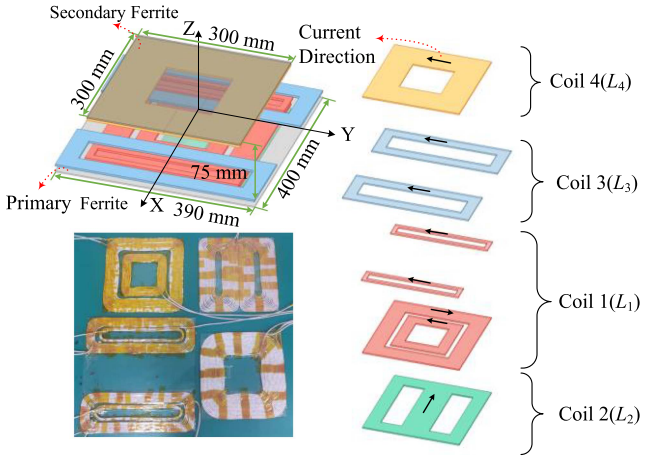

Fig. 2. Proposed coil structure.

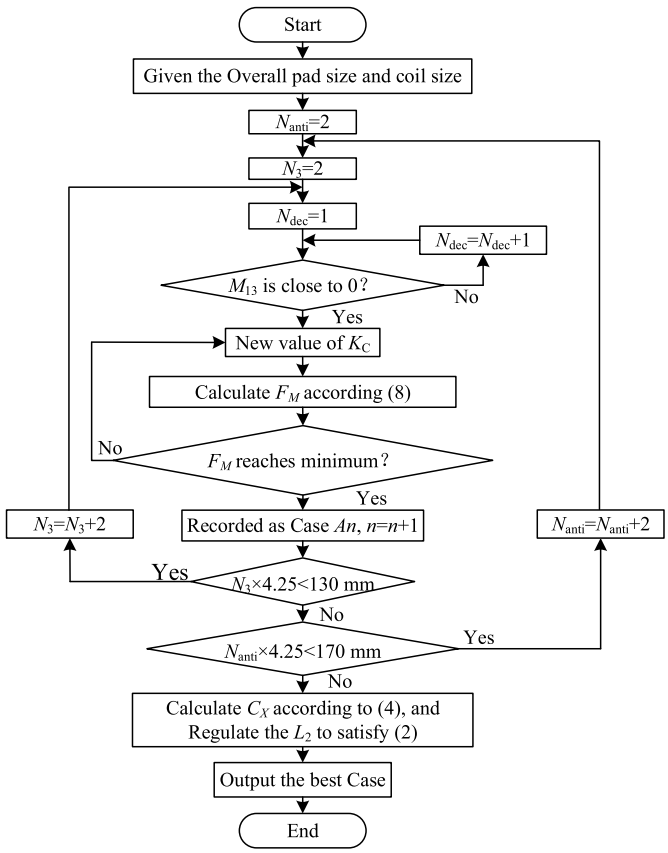

Fig. 3. Design flow for magnetic couplers and K_C.

In order to determine the appropriate turn numbers for the magnetic couplers, a design flow is proposed, as shown in Fig. 3. The transmitting coil sizes are set to 390 × 400 mm. The turn numbers of the antiparallel winding N_{anti} and the decoupling windings N_{dec} and N_3 should be optimized. K_C changes with the turn numbers and there exists a minimum value. Thus, K_C is taken into account in the flowchart.

The designed transmitting coils are shown in Fig. 4. The turn number of the decoupling winding is 3. The coupling coefficient

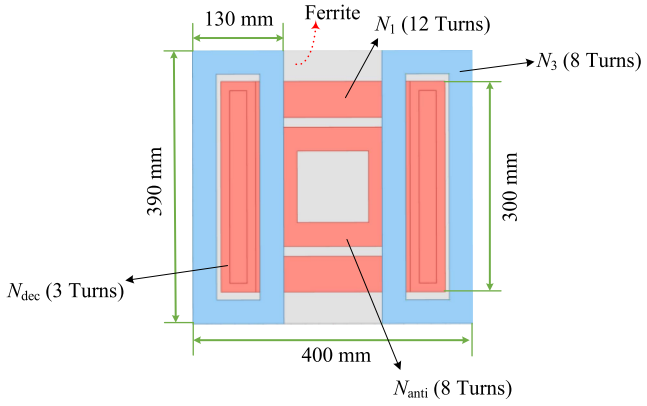

Fig. 4. Top view of the three coils on the primary side.

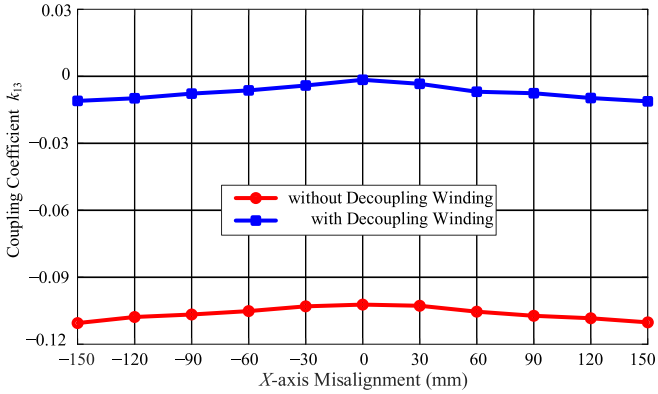

Fig. 5. Simulated coupling coefficient of k_{13} with and without decoupling windings.

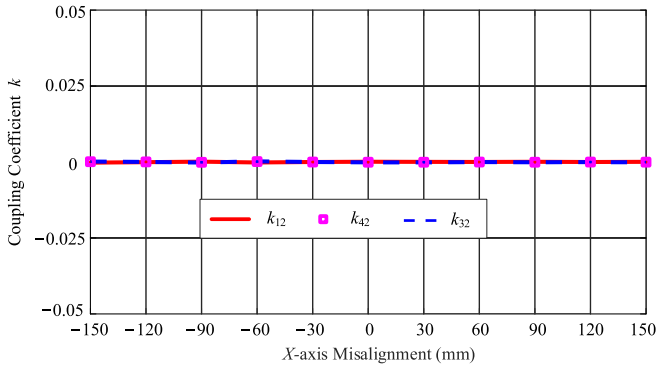

Fig. 6. Simulated coupling coefficients between L_2 and other coils varying with *X*-axis misalignment.

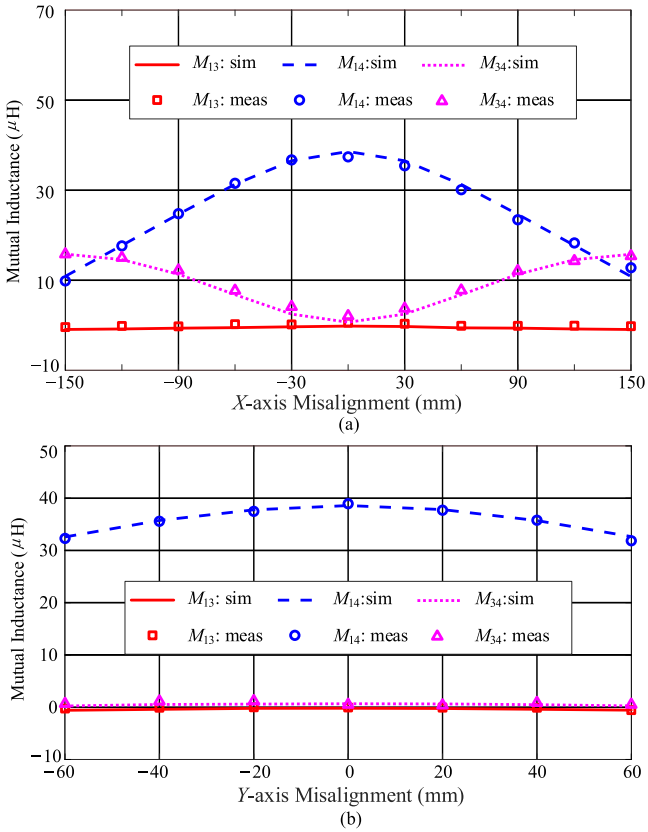

Fig. 7. Simulated and measured mutual inductances varying with misalignments. (a) *X*-axis direction. (b) *Y*-axis direction.

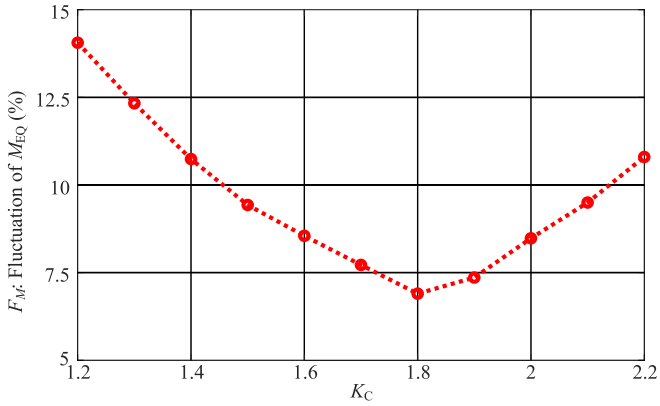

Fig. 8. Fluctuation of M_{EQ}, or F_M, varying with K_C.

between L_1 and L_3 (k_{13}) varying with the *X*-axis misalignment, which is set as the door–door direction, with and without the decoupling winding is shown in Fig. 5. k_{13} has decreased significantly from 0.1 to less than 0.01. This means that L_1 and L_3 can be regarded as decoupled. The reason for decoupling L_1 and L_3 is that k_{13} will cause the input impedance to have an imaginary part, resulting in a large reactive power and losing the ZPA operation.

Fig. 6 presents the coupling coefficients between Coil 2 and the other three coils. They are maintained at 0, indicating that decoupling has been achieved.

The simulated and measured mutual inductances varying with the *X*-axis and *Y*-axis misalignments are shown in Fig. 7. The range of the *X*-axis misalignment is set at 150 mm, half the length of the receiving coil. With the increasing *X*-axis misalignment, M_{14} decreases gradually and M_{34} behaves oppositely. The range

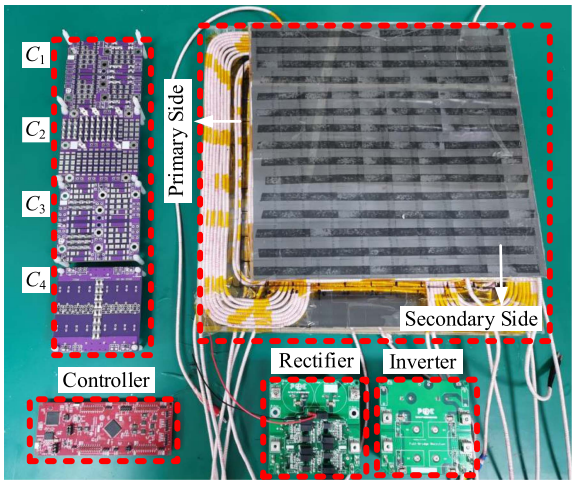

Fig. 9. Photograph of the experimental prototype.

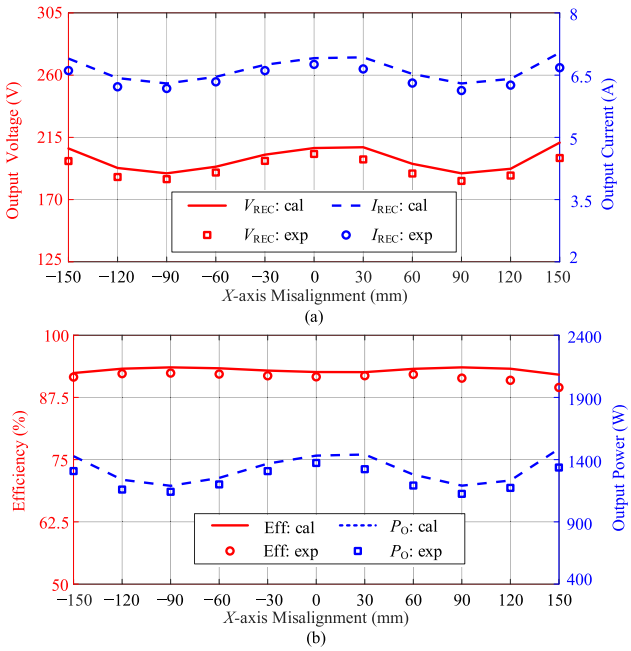

Fig. 10. Calculations and experimental results with X-axis misalignment. (a) Output voltage and output current. (b) Efficiency and output power.

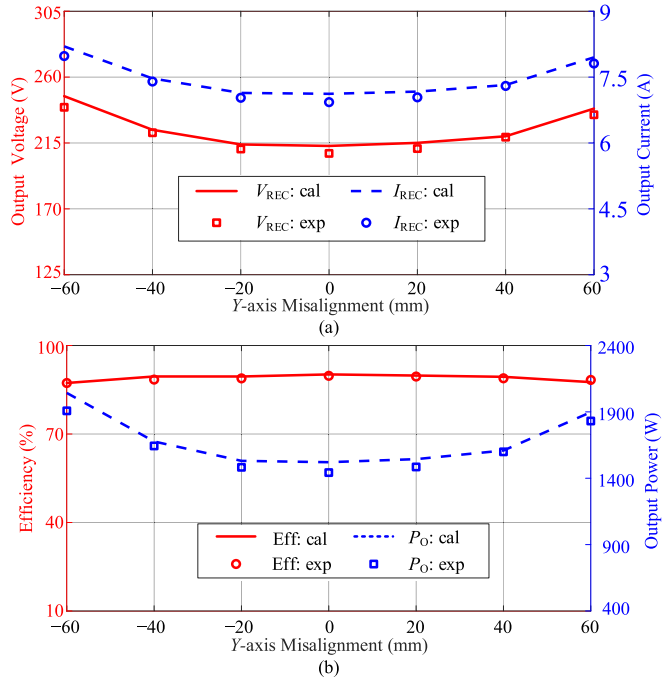

Fig. 11. Calculations and experimental results with the Y-axis misalignment. (a) Output voltage and output current. (b) Efficiency and output power.

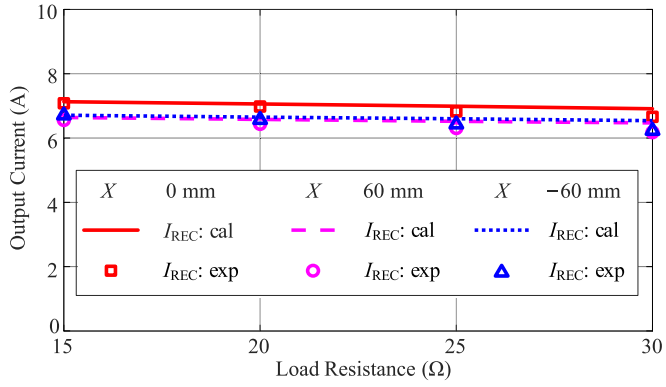

Fig. 12. Calculations and experimental results of output current varying with R_L.

of the Y-axis misalignment is set at 60 mm. With the increasing Y-axis misalignment, M_{14} decreases gradually, while M_{34} remains at 0.

Because M_{14} and M_{34} are two monotonically changing curves with opposite directions within the misalignment range, there would be a minimum point of F_M. The fluctuation of M_{EQ}, or F_M, varying with K_C is depicted in Fig. 8. When K_C is equal to 1.8, F_M is minimized. Thus, K_C is set to 1.8.

III. Experimental Validation

To verify the feasibility of the LC squared-compensated IPT system, a 1.3-kW prototype is built, as shown in Fig. 9. The parameters of the prototype are given in Table I. The Chroma 62150H-600 dc power supplies and the ITECH IT8906E-600-420 are used as the dc source and the electronic load, respectively. The Tektronix MSO 46 oscilloscope is used to capture the voltage and current waveforms at the input and output ends of the magnetic coupler.

The X-axis misalignment of the receiving coil is set from −150 to 150 mm to evaluate the misalignment performance.

TABLE I
Parameters of Experimental Prototype

Parameter	Value	Parameter	Value	Parameter	Value
L_1 (μH)	105.58	C_1 (nF)	34.15	V_{INV} (V)	200
L_2 (μH)	161.68	C_2 (nF)	63.45	f (kHz)	85
L_3 (μH)	67.34	C_3 (nF)	312.3	R_{L} (Ω)	30
L_4 (μH)	199	C_4 (nF)	17.55	-	-

TABLE II
COMPARISONS WITH EXISTING METHODS

Ref.	Number of Compensation Capacitor	Number of Compensation Inductor	Secondary-Side Compensation Topology	Door-Door Misalignment (mm)	Receiver Coil Length (mm)	Load-Independent Output	Rated Power (kW)	Efficiency (%)	Output Fluctuation (%)
[19]	5	None	S and LCC	300	600	CC	3.3	95.6	5
[27]	4	2	CLLLC	200	400	CC	3.5	96.31	5
[28]	6	None	S and LCC	70	240	CC	0.25	94.3	5.6
[29]	4	2	LCC	180	400	CC	3	92	1.5
[30]	6	2	S and LCC	200	400	CV	3.5	94.5	5
This article	4	1	S	150	300	CC	1.3	91.6	5

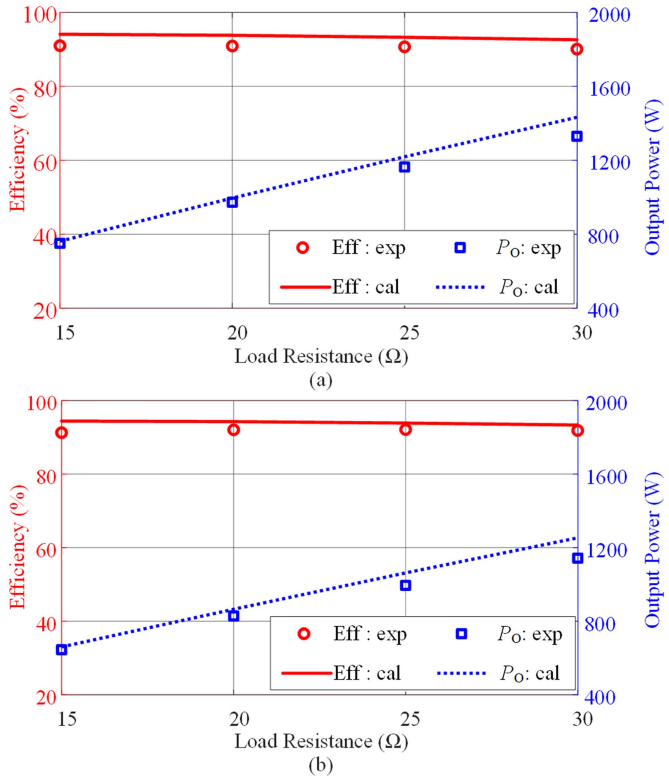

Fig. 13. Calculations and experimental results of output power and efficiency varying with R_L. (a) $X = 0$ mm and $Y = 0$ mm. (b) $X = 60$ mm and $Y = 0$ mm.

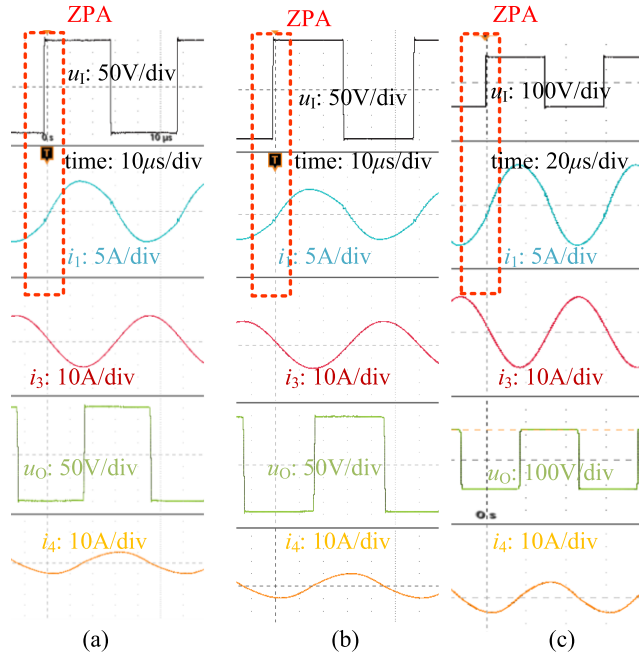

Fig. 14. Experimental waveforms with different R_L and misalignment distance. (a) $X = 0$ mm, $Y = 0$ mm, and $R_L = 30\ \Omega$. (b) $X = -60$ mm, $Y = 0$ mm, and $R_L = 25\ \Omega$. (c) $X = 0$ mm, $Y = 60$ mm, and $R_L = 30\ \Omega$.

The calculated and experimental results of the output voltage, the output current, the output power, and the dc–dc efficiency varying with the X-axis misalignment when $R_L = 30\ \Omega$ are shown in Fig. 10. The measured results match well with the calculations. The maximum and minimum values of the output voltage are 203 V and 183 V, respectively. The system can deliver 1373 W with a dc–dc efficiency of 91.6% under the best position of $X = 0$ mm and 1235 W with a 92.3% dc–dc efficiency under the position of $X = 90$ mm. The corresponding maximum and minimum values of the output currents are 6.76 A and 6.13 A,

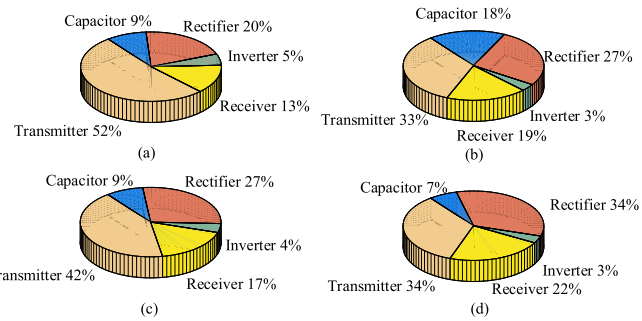

Fig. 15. Loss breakdown. (a) $X = 0$ mm and $R_L = 30\ \Omega$. (b) $X = 0$ mm and $R_L = 20\ \Omega$. (c) $X = -60$ mm and $R_L = 25\ \Omega$. (d) $X = -60$ mm and $R_L = 20\ \Omega$.

respectively. The fluctuation of the output current, obtained from (8), is about 5%. The efficiency is maintained at 90%. Based on the verifications mentioned above, it is obvious that the system is robust to the door–door direction to achieve a stable output.

The calculated and experimental results of the output voltage, the output current, the output power, and the dc–dc efficiency varying with the Y-axis misalignment when $R_L = 30\ \Omega$ are shown in Fig. 11. The measured results match well with the calculations. The system can deliver 1908 W under the $Y = 60$ mm.

To validate the CC output characteristic, R_L is varied. The calculated and experimental results of the output current are given in Fig. 12. The output current fluctuation is less than 2%, which is acceptable considering the influence of measurement errors and the ESRs. The output current remains constant with the varying load resistance under misalignment. The dc–dc efficiency and the output power varying with the load resistance under different misalignment cases are depicted in Fig. 13, which demonstrates that the efficiency remains consistent at approximately 90% for all the cases. As the load resistance increases, the output power also increases linearly.

The experimental waveforms of the three cases are shown in Fig. 14. It can be seen that ZPA has been achieved.

For the proposed IPT system, the system losses mainly include the inverter losses, the compensation capacitor losses, the transmitter coil losses, the receiver coil losses, and the rectifier losses. Fig. 15 shows the distribution of the system losses for four operating conditions. The largest percentage of losses is dissipated in the IPT coils.

The comparisons between this work and existing works are shown in Table II. The proposed system can achieve similar misalignment tolerance performance with a smaller number of compensation components. Also, the secondary-side compensation topology is simple with the series compensation requiring only one compensation capacitor. However, the lack of the misalignment tolerance in the Y-axis direction is the major disadvantage of the proposed system, which needs further research and improvement.

IV. Conclusion

This article has proposed an IPT system with the secondary-side series compensation and the primary-side LC squared compensation to realize misalignment tolerance and a CC output. The series compensation is adopted on the secondary side for a compact receiver. The three coils on the primary side are integrated and decoupled from each other, with the first and third coils coupled with the receiving coil. The mathematical model has been developed and the equivalent mutual inductance has been derived. The misalignment tolerance performance and the CC output have been analyzed. A design flow has been provided to guarantee the misalignment tolerance performance of the proposed IPT system. A 1.3-kW experimental prototype has been implemented to verify the effectiveness of the proposed IPT system. The dc–dc efficiency of 91.6% has been achieved while delivering 1373 W to the load in a fully aligned position. The output current fluctuation is less than 5%. The output current at the light and rated load is 7.13 A and 6.91 A, respectively. The misalignment tolerance and the CC output of the proposed LC squared-compensated IPT system have been successfully realized.

The advantage of the proposed LC squared-compensated IPT system is that it achieves relatively high misalignment tolerance performance with few compensation components, especially on the secondary side. The proposed IPT system is a low-cost solution to achieve door–door misalignment tolerance and CC charging.

References

[1] Y. Zhang, Z. Shen, W. Pan, H. Wang, Y. Wu, and X. Mao, "Constant current and constant voltage charging of wireless power transfer system based on three-coil structure," *IEEE Trans. Ind. Electron.*, vol. 70, no. 1, pp. 1066–1070, Jan. 2023.

[2] Y. Wang, T. Li, M. Zeng, J. Mai, P. Gu, and D. Xu, "An underwater simultaneous wireless power and data transfer system for AUV with high-rate full-duplex communication," *IEEE Trans. Power Electron.*, vol. 38, no. 1, pp. 619–633, Jan. 2023.

[3] Y. Zhang et al., "A quadrupole receiving coil with series-connected diode rectifiers for interoperability of nonpolarized and polarized transmitting coils," *IEEE Trans. Power Electron.*, vol. 38, no. 7, pp. 8000–8004, Jul. 2023.

[4] Y. Wu, H. Wang, Y. Zhuang, and Y. Zhang, "A shared charging channel for power and auxiliary batteries in electric vehicles," *IEEE Trans. Ind. Electron.*, to be published, doi: 10.1109/TIE.2023.3312435.

[5] R. Xie, R. Liu, X. Chen, X. Mao, X. Li, and Y. Zhang, "An interoperable wireless power transmitter for unipolar and bipolar receiving coils based on three-switch dual-output inverter," *IEEE Trans. Power Electron.*, vol. 39, no. 2, pp. 1985–1989, Feb. 2024.

[6] S. Wu, C. Cai, A. Wang, Z. Qin, and S. Yang, "Design and implementation of a uniform power and stable efficiency wireless charging system for autonomous underwater vehicles," *IEEE Trans. Ind. Electron.*, vol. 70, no. 6, pp. 5674–5684, Jun. 2023.

[7] Z. Yan et al., "Free-rotation wireless power transfer system based on composite anti-misalignment method for AUVs," *IEEE Trans. Power Electron.*, vol. 38, no. 4, pp. 4262–4266, Apr. 2023.

[8] C. Rong et al., "Optimization design of resonance coils with high misalignment tolerance for drone wireless charging based on genetic algorithm," *IEEE Trans. Ind. Appl.*, vol. 58, no. 1, pp. 1242–1253, Jan./Feb. 2022.

[9] J. Kim et al., "A proposed fast charging and high-power system for wireless railway trains adopting the input voltage sharing topology and the balancing control scheme," *IEEE Trans. Ind. Electron.*, vol. 67, no. 8, pp. 6407–6417, Aug. 2020.

[10] E. Rong, P. Sun, K. Qiao, X. Zhang, G. Yang, and X. Wu, "Six-plate and hybrid-dielectric capacitive coupler for underwater wireless power transfer," *IEEE Trans. Power Electron.*, vol. 39, no. 2, pp. 2867–2881, Feb. 2024.

[11] Y. Wu, C. Liu, M. Zhou, X. Mao, and Y. Zhang, "An antioffset electric vehicle wireless charging system based on dual coupled antiparallel coils," *IEEE Trans. Power Electron.*, vol. 38, no. 5, pp. 5634–5637, May 2023.

[12] Y. Zhang, C. Liu, M. Zhou, and X. Mao, "A novel asymmetrical quadrupolar coil for interoperability of unipolar, bipolar, and quadrupolar coils in electric vehicle wireless charging systems," *IEEE Trans. Ind. Electron.*, vol. 71, no. 4, pp. 4300–4303, Apr. 2024.

[13] E. Gati, G. Kampitsis, and S. Manias, "Variable frequency controller for inductive power transfer in dynamic conditions," *IEEE Trans. Power Electron.*, vol. 32, no. 2, pp. 1684–1696, Feb. 2017.

[14] C. Xia, W. Wang, S. Ren, X. Wu, and Y. Sun, "Robust control for inductively coupled power transfer systems with coil misalignment," *IEEE Trans. Power Electron.*, vol. 33, no. 9, pp. 8110–8122, Sep. 2018.

[15] A. Hossain, P. Darvish, S. Mekhilef, K. S. Tey, and C. W. Tong, "A new coil structure of dual transmitters and dual receivers with integrated decoupling coils for increasing power transfer and misalignment tolerance of wireless EV charging system," *IEEE Trans. Ind. Electron.*, vol. 69, no. 8, pp. 7869–7878, Aug. 2022.

[16] Y. Wang, H. Liu, F. Wu, P. Wheeler, Q. Zhou, and S. Zhao, "Research on a three-coil hybrid IPT charger with improved tolerance to coupling variation and load-independent output," *IEEE J. Emerg. Sel. Topics Ind. Electron.*, vol. 4, no. 2, pp. 625–636, Apr. 2023.

[17] Y. Zhang, S. Chen, X. Li, and Y. Tang, "Design methodology of free-positioning nonoverlapping wireless charging for consumer electronics based on antiparallel windings," *IEEE Trans. Ind. Electron.*, vol. 69, no. 1, pp. 825–834, Jan. 2022.
[18] L. Xu, Q. Chen, X. Ren, S.-C. Wong, and C. K. Tse, "Self-oscillating resonant converter with contactless power transfer and integrated current sensing transformer," *IEEE Trans. Power Electron.*, vol. 32, no. 6, pp. 4839–4851, Jun. 2017.
[19] G. Li, Z. Yao, S. Luo, and H. Ma, "A hybrid IPT system implementing misalignment tolerance and constant current output with primary intermediate coil," *IEEE J. Emerg. Sel. Topics Power Electron.*, vol. 10, no. 6, pp. 7797–7807, Dec. 2022.
[20] Y. Chen et al., "A clamp circuit-based inductive power transfer system with reconfigurable rectifier tolerating extensive coupling variations," *IEEE Trans. Power Electron.*, vol. 39, no. 2, pp. 1942–1946, Feb. 2024.
[21] L. Zhao, D. J. Thrimawithana, and U. K. Madawala, "Hybrid bidirectional wireless EV charging system tolerant to pad misalignment," *IEEE Trans. Ind. Electron.*, vol. 64, no. 9, pp. 7079–7086, Sep. 2017.
[22] Y. Chen et al., "Reconfigurable topology for IPT system maintaining stable transmission power over large coupling variation," *IEEE Trans. Power Electron.*, vol. 35, no. 5, pp. 4915–4924, May 2020.
[23] H. Feng, T. Cai, S. Duan, J. Zhao, X. Zhang, and C. Chen, "An LCC-compensated resonant converter optimized for robust reaction to large coupling variation in dynamic wireless power transfer," *IEEE Trans. Ind. Electron.*, vol. 63, no. 10, pp. 6591–6601, Oct. 2016.
[24] Y. Zhang et al., "Misalignment-tolerant dual-transmitter electric vehicle wireless charging system with reconfigurable topologies," *IEEE Trans. Power Electron.*, vol. 37, no. 8, pp. 8816–8819, Aug. 2022.
[25] C. Cai, X. Liu, S. Wu, X. Chen, W. Chai, and S. Yang, "A misalignment tolerance and lightweight wireless charging system via reconfigurable capacitive coupling for unmanned aerial vehicle applications," *IEEE Trans. Power Electron.*, vol. 38, no. 1, pp. 22–26, Jan. 2023.
[26] Y. Zhang et al., "Passive paralleling of multi-phase diode rectifier for wireless power transfer systems," *IEEE Trans. Circuits Syst. II, Express Briefs*, vol. 70, no. 2, pp. 646–649, Feb. 2023.
[27] B. Yang, Y. Chen, W. Ruan, H. Liu, Y. Ren, and R. Mai, "Current stress optimization for double-sided CLLLC topology-based IPT system with constant output current tolerating pad misalignments," *IEEE Trans. Ind. Appl.*, vol. 58, no. 1, pp. 1032–1043, Jan./Feb. 2022.
[28] G. Ke, Q. Chen, L. Xu, X. Ren, and Z. Zhang, "Analysis and optimization of a double-sided S-LCC hybrid converter for high misalignment tolerance," *IEEE Trans. Ind. Electron.*, vol. 68, no. 6, pp. 4870–4881, Jun. 2021.
[29] Y. Chen, R. Mai, Y. Zhang, M. Li, and Z. He, "Improving misalignment tolerance for IPT system using a third-coil," *IEEE Trans. Power Electron.*, vol. 34, no. 4, pp. 3009–3013, Apr. 2019.
[30] Y. Chen et al., "A hybrid inductive power transfer system with misalignment tolerance using quadruple-D quadrature pads," *IEEE Trans. Power Electron.*, vol. 35, no. 6, pp. 6039–6049, Jun. 2020.
[31] H. Tang, Z. Shen, Z. Huang, H. Zhou, S. Chen, and Y. Zhang, "An LCC2-S compensated IPT system for misalignment tolerance with a compact receiver," in *Proc. IECON - 49th Annu. Conf. IEEE Ind. Electron. Soc.*, 2023, pp. 1–4.

Yiming Zhang (Senior Member, IEEE) received the B.S. and Ph.D. degrees in electrical engineering from Tsinghua University, Beijing, China, in 2011 and 2016, respectively.

Afterward, he was a Postdoctoral Researcher with San Diego State University, San Diego, CA, USA, and a Research Fellow with Nanyang Technological University, Singapore. He is currently a Full Professor with Fuzhou University, Fuzhou, China. He has authored 1 book from Springer, and authored or coauthored more than 100 technical papers in journals and conference proceedings. His research interests include wireless power transfer and resonant converters.

Dr. Zhang was the recipient of the Outstanding Doctoral Dissertations of Tsinghua University in 2016. He was recognized as an Outstanding Reviewer of IEEE TRANSACTIONS ON POWER ELECTRONICS in 2019 and 2022, and a Distinguished Reviewer of IEEE TRANSACTIONS ON INDUSTRIAL ELECTRONICS in 2020. He was the Publication Chair of the International Conference ICWPT2022.

Hongmin Tang was born in Fujian, China. He is currently working toward the master's degree in electrical engineering in power electronics with the School of Electrical Engineering and Automation, Fuzhou University, Fuzhou, China.

His research interests include wireless power transfer.

Zhiwei Shen was born in Nanping, China. He is currently working toward the master's degree in electrical engineering in power electronics with the School of Electrical Engineering and Automation, Fuzhou University, Fuzhou, China.

His research direction includes wireless power transfer.

Yizhan Zhuang (Member, IEEE) was born in Fujian, China, in 1994. He received the B.S. degree from the College of Electrical Engineering and Automation, Fuzhou University, Fuzhou, China, in 2017, and the Ph.D. degree from the School of Electrical Engineering, Wuhan University, Wuhan, China, in 2023.

He is currently a Lecturer (Associate Researcher) with the School of Electrical Engineering and Automation, Fuzhou University, Fuzhou, China. His research interests include dc–dc power converter and interface of photovoltaic conversion systems.

Zhongqi Li (Member, IEEE) was born in Yueyang in 1985. He received the M.Sc. degree from the Hunan University of Technology, Zhuzhou, China, in 2012, and the Ph.D. degree from Hunan University, Changsha, China, in 2016.

Since 2016, he has been an Associate Professor with the Hunan University of Technology, China. Since 2020, he has been a Postdoctoral Fellow with Hunan University. His research interests include wireless power transfer systems and soft-switching power converters.